Stockholm University

Turbulence and Shell Models of Helical and Non-helical Chiral MHD

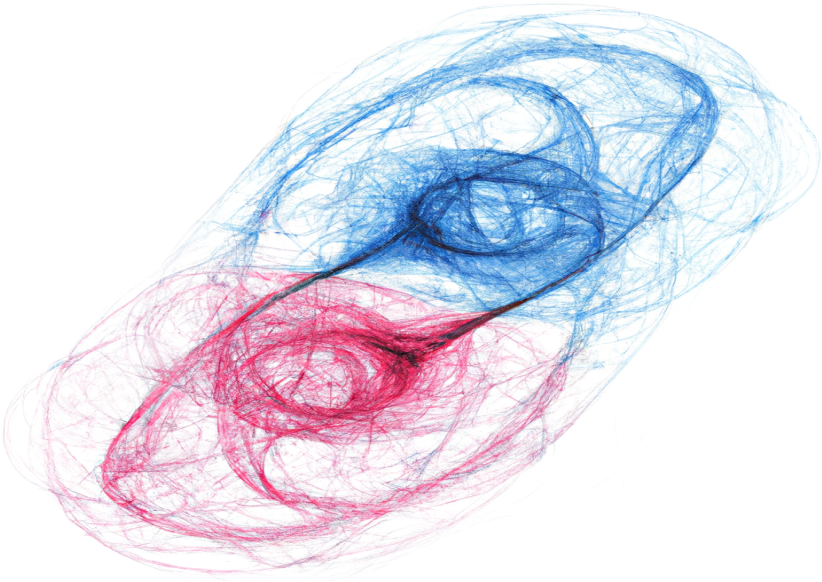

Cover image: AI generated picture of two merging helicity structures with opposite sign.

Student: Gustav Larsson
Supervisor: Axel Brandenburg

Abstract

In both hydrodynamics as well as in magnetohydrodynamics (MHD) conserved quantities plays a governing role in the evolution of the fields. We investigate these quantities and their role in the decay of magnetic turbulence. We present the underlying theory of chiral MHD as well as the non-helical cases when the total averaged helicity is zero. We discuss the newly introduced Hosking integral and its consequences. The MHD equations are solved by using Shell models which can cover enormous ranges using logarithmically spaced wave numbers. From the scaling of the decay we can test the precision of the shell models by comparing them with direct numerical simulations.

List of Papers

The following paper are included in this thesis.

PAPER I: **Turbulence with Magnetic Helicity that is Absent on Average**
Axel Brandenburg, Gustav Larsson, **Turbulence from Earth to Planets, Stars and Galaxies—Commemorative Issue Dedicated to the Memory of Jackson Rae Herring**, *Atmosphere*,14, 932 (2023).
DOI: 10.3390/atmos14060932

Contents

List of Figures

Acknowledgements

First and foremost, I would like to express my deepest gratitude to my supervisor Axel Brandenburg for his invaluable supervision, immense knowledge, guidance and motivation. This journey would not have been possible without him. I am also thankful to Yutong He, Ramkishor Sharma and Salome Mtchedlidze for their kind help and support.

1. Introduction

In magnetohydrodynamic (MHD) turbulence, the presence of certain conservation laws explains the phenomenon of an inverse cascade which causes a growth of magnetic energy to larger scales as energy decays [3]. In the presence of chiral fermions with a chiral chemical potential μ_5, there is an instability that leads to the inverse cascade. The chiral chemical potential is a quantum effect which occurs due to an asymmetry between left and right-handed fermions. This leads to a proportionality between the current density and the magnetic field which adds an additional term proportional to μ_5 to the induction equation and leads to a dynamo effect [5]. The range of the subinertial inverse cascade is often several orders of magnitudes apart. This requires numerical methods. We are here dealing with partial differential equations with no possibility to analytical solutions. Therefore we solve the MHD equations through the shell model of turbulence which couples the evolution of each k to its nearest neighbour. This enables us to do numerical calculations of enormous wavenumbers using logarithmically spaced wave numbers $k_n = k_1 2^n$ with $0 \leq n \leq 30$. With $N = 30$, we can obtain ranges up to ten orders of magnitude in wavenumber [4]. The shell model is not an approximation and should rather be treated as a TOY model that has similar conservation laws as the MHD equations [6].

In hydrodynamics there is no inverse cascade of energy due to the conservation of certain invariants. This is not the case in MHD where the conserved magnetic helicity can lead to a cascade of energy to larger length scales as energy decays. In the absence of total averaged helicity it was believed that there should be no inverse cascade. But numerical simulations showed the opposite [4]. The explanation of an inverse cascade in the absence of total averaged helicity became clear in 2021 when the Hosking integral was introduced [7]. In this report we explain the arguments leading to an inverse cascade both in the case of finite chirality and when the total averaged helicity is zero. The decay behaviours of turbulent magnetic fields are determined by these quantities. We present dimensional arguments that allows us to determine the scaling of their decay behaviours and from these scaling we can test the shell models[4].

2. Theoretical background

In different astrophysical scenarios the plasma is considered fully ionized [1]. Due to the movement of charged particles this leads to the creation of magnetic fields. The interaction between the ionized plasma and the magnetic fields is what is studied in magnetohydrodynamics. The MHD equations are derived from Maxwell's equations,

$$\frac{\partial \boldsymbol{B}}{\partial t} = -\boldsymbol{\nabla} \times \boldsymbol{E}, \tag{2.1}$$

$$\frac{1}{c^2}\frac{\partial \boldsymbol{E}}{\partial t} = \boldsymbol{\nabla} \times \boldsymbol{B} - \mu_0 J, \tag{2.2}$$

$$\boldsymbol{\nabla} \cdot \boldsymbol{E} = \frac{\rho_e}{\varepsilon_0}. \tag{2.3}$$

Usually Ohm's law tells us how the current density is related to the force acting on free charges in a medium and is given by, $\boldsymbol{J} = \sigma \boldsymbol{E}$ [8]. This is also true in MHD but only that here we need to consider the electric field in a co-moving frame with the velocity of the plasma, which leads to Ohm's law written on the form,

$$\boldsymbol{J} = \sigma \boldsymbol{E}_{\text{comov}} = \sigma(\boldsymbol{E} + \boldsymbol{u} \times \boldsymbol{B}), \tag{2.4}$$

where $\boldsymbol{E}_{\text{comov}}$ is denoting that it is co-moving with the frame and is given by,

$$\boldsymbol{E}_{\text{comov}} = \boldsymbol{E} + \boldsymbol{u} \times \boldsymbol{B}. \tag{2.5}$$

In the situations consider in this report the Maxwell displacement current in Equation (2.2) can be neglected. This is because in the cases we consider the velocities are small compared to the speed of light [8]. To demonstrate this we can look at the charge conservation [8],

$$\boldsymbol{\nabla} \cdot \boldsymbol{J} = -\frac{\partial \rho_{\text{e}}}{\partial t}, \tag{2.6}$$

and the divergence of Equation (2.4) together with Gauss' law applied on Equation (2.6),

$$\frac{\partial \rho_{\text{e}}}{\partial t} + \frac{\rho_{\text{e}}}{\tau_{\text{e}}} + \sigma \boldsymbol{\nabla} \cdot (\boldsymbol{u} \times \boldsymbol{B}) = 0. \tag{2.7}$$

The quantity $\tau = \varepsilon_0/\sigma$ is the relaxation time and is very small, approximately $10^{-18}s$ which allows us to neglect the first term in Equation (2.7) These arguments also implies that the Faraday displacement current in Equation (2.2) can be neglected since,

$$\varepsilon_0 \frac{\partial \boldsymbol{E}}{\partial t} \sim \frac{\varepsilon_0}{\sigma} \frac{\partial \boldsymbol{J}}{\partial t} \sim \tau_e \frac{\partial \boldsymbol{J}}{\partial t} \ll \boldsymbol{J}. \tag{2.8}$$

This gives us $\boldsymbol{J} = \boldsymbol{\nabla} \times \boldsymbol{B}/\mu$, which together with Ohms law can be substituted in Equation (2.1)[8],

$$\frac{\partial \boldsymbol{B}}{\partial t} = \boldsymbol{\nabla} \times (\boldsymbol{u} \times \boldsymbol{B}) + \eta \nabla^2 \boldsymbol{B}. \tag{2.9}$$

Which is the induction equation and it tells us about the evolution of the magnetic field and the velocity of the conducting plasma [1]. Here we use Heaviside–Lorentz units so that, μ and $c = 1$, η is the magnetic diffusivity, $\eta = \frac{1}{\mu_0 \sigma}$ and $\boldsymbol{u}$ is the velocity field of the plasma. One could argue that a better name for the induction equation would be the advection-diffusion equation. To understand this we need to go back to fluid mechanics. In fluid mechanics different flows are studied depending on the viscosity and the speed of the field flow [8]. High viscosity and low speed flows is categorized in what is called laminar flow, meaning organized. In this report and in most of the realistic scenarios, with flows of normal speed, the flows are very sensitive to perturbations which causes the flow to be chaotic or turbulent [8]. The different flows are determined by the so called Reynolds number. Here we are interested in the magnetic Reynolds number R_m which is given by the ratio of the two terms in Equation (2.9). The first term is the convective term of the magnetic field by the velocity field and the second term is the diffusive term. Where the ratio between the two terms is defined as the magnetic Reynolds number R_m and is a measure of the induction. From dimensional arguments we get,

$$R_m = \frac{Lu}{\eta}. \tag{2.10}$$

In this report we consider magnetic Reynolds numbers around the order of 1000 [1]. The seed magnetic fields can be amplified exponentially by dynamo effects as in the alpha effect where an instability in the induction equation occurs due to the helicity of magnetic fields [1].

2.1 Helicity

Magnetic helicity is defined as,

$$H = \int_V \boldsymbol{A} \cdot \boldsymbol{B} \ dV. \tag{2.11}$$

Where $\boldsymbol{A}$ is the vector potential and $\boldsymbol{B}$ the magnetic field. The integral is defined as the volume over a closed box. The physical meaning of helicity is the twisting and linkage of the magnetic fields [1]. This can be seen by looking at the net helicity of two interlocked flux tubes ϕ_1 and ϕ_2 shown in Figure 2.1.

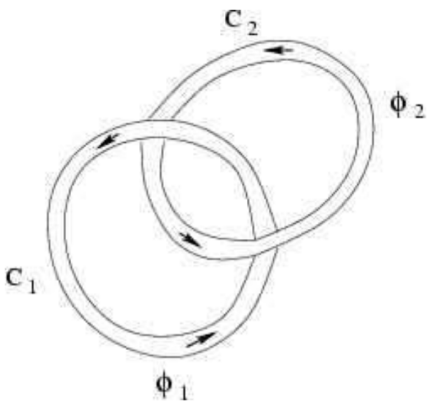

Figure 2.1: Two interlocked helicity flux tubes. Figure credit [1].

Here C_1 and C_2 is tube 1 and 2 respectively and V_1 and V_2 is their volumes. We can now calculate the flux through the cross section of the flux tubes by splitting the integral in Equation (2.11) and add their contributions,

$$H = \int_{L_1} \boldsymbol{A} \cdot dl \int_{S_1} \boldsymbol{B} \cdot ds + \int_{L_2} \boldsymbol{A} \cdot dl \int_{S_2} \boldsymbol{B} \cdot ds, \tag{2.12}$$

by using Stokes theorem we can rewrite Equation (2.12) as,

$$\oint_{C_1} \boldsymbol{A} \cdot dl = \int_{S(C_1)} \boldsymbol{B} \cdot ds \equiv \phi_2, \tag{2.13}$$

which leads to,

$$H = \phi_1 \oint_{C_1} \boldsymbol{A} \cdot dl + \phi_2 \oint_{C_2} \boldsymbol{A} \cdot dl = \pm 2\phi_1\phi_2. \tag{2.14}$$

Magnetic helicity is conserved in ideal MHD. This can be seen by looking at the evolution equation which is derived from the uncurled version of Faraday's law,

$$\frac{\partial \boldsymbol{A}}{\partial t} = -\boldsymbol{E} - \boldsymbol{\nabla}\phi, \tag{2.15}$$

where $\boldsymbol{\nabla}\phi$ is the scalar potential which is needed for gauge invariance. By using Equation (2.15) we can find the evolution of H as,

$$\frac{\partial(\boldsymbol{A}\cdot\boldsymbol{B})}{\partial t} = (-\boldsymbol{E} + \boldsymbol{\nabla}\phi)\cdot\boldsymbol{B} + \boldsymbol{A}\cdot(-\boldsymbol{\nabla}\times\boldsymbol{E}) = -2\boldsymbol{E}\cdot\boldsymbol{B} + \boldsymbol{\nabla}\cdot(\phi\boldsymbol{B} + \boldsymbol{A}\times\boldsymbol{E}). \tag{2.16}$$

Now by integrating Equation (2.16) over a volume V and using Stokes theorem we get,

$$\frac{dH}{dt} = -2\int_V \boldsymbol{E}\cdot\boldsymbol{B}\ \ dV + \oint_{\partial V}(\boldsymbol{A}\times\boldsymbol{E}+\phi\boldsymbol{B})\cdot\hat{\boldsymbol{n}}dS = -2\eta C. \tag{2.17}$$

Here we have assumed that the second term is zero and $C = \int_V J\cdot B\ \ dV$ is defined as the current helicity. In ideal MHD the diffusivity, $\eta = 0$. This might seem non-realistic. But it turns out that in cases with high magnetic Reynolds number, the diffusivity is negligible and helicity is therefore conserved [1].

2.2 Helicity spectra

The normalized spectra of the magnetic energy and helicity is obtained by Fourier transforming the correlation functions. This applies to all the spectra presented in this paper (See [8] for more details). The different spectra is given by,

$$\int_0^\infty E_M(k)\ \ dk = \langle\frac{1}{2}\boldsymbol{B}^2\rangle V \equiv E_M, \tag{2.18}$$

$$\int_0^\infty H_M(k)\ \ dk = \langle\boldsymbol{A}\cdot\boldsymbol{B}\rangle V \equiv H_M. \tag{2.19}$$

Where V is the volume of integration [1]. The normalized spectra can be written as,

$$E_M(k) = \frac{1}{2}\frac{\langle\boldsymbol{B_k^2}\rangle V}{\delta_k}, \tag{2.20}$$

$$H_M(k) = \frac{\langle\boldsymbol{A_k}\cdot\boldsymbol{B_k}\rangle V}{\delta_k}. \tag{2.21}$$

The different spectra is often rewritten by a decomposing the Fourier transformed magnetic vector potential and complex coefficients $a_k^\pm$, which leads to (See [1] for more details),

$$E_M(k) = \tfrac{1}{2}k^2(|a_k^+|^2+|a_k^-|^2)V, \tag{2.22}$$

$$H_M(k) = k(|a_k^+|^2-|a_k^-|^2)V. \tag{2.23}$$

By multiplying Equation (2.23) with $k/2$ and applying a Cauchy-Schwarz type inequality on Equation (2.22) and Equation (2.23) we obtain,

$$\tfrac{1}{2}k^2(|a_k^+|^2+|a_k^-|^2)V \geq \tfrac{1}{2}k^2(|a_k^+|^2-|a_k^-|^2)V, \tag{2.24}$$

which leads to,

$$\frac{1}{2}k|H(k)| \leq E_M(k). \tag{2.25}$$

This is the so called realizability condition [1]. In the fully helical case it is given by,

$$E_M(k) = \pm\frac{1}{2}k|H(k)|. \tag{2.26}$$

This argument is crucial for the inverse cascade which transfers energy from smaller to larger scales and will be demonstrated later [1].

2.3 Forward cascade

As mentioned above, a possibility to produce large scale magnetic fields is by a so called inverse cascade [1]. A forward cascade was explained by Richardson and Kolmogorov and tells us how larger eddies transport energy to larger wavenumbers via smaller and smaller eddies [8]. In this case the energy spectra is given by,

$$\frac{1}{2}\langle \boldsymbol{u}^2 \rangle = \int E(k)dk, \tag{2.27}$$

where $\boldsymbol{u}$ is the velocity field.

In the inertial subrange shown in Figure 2.2 Kolmogorov came up with an energy spectra on the form,

$$E(k) = C\mathcal{E}^{\frac{2}{3}}k^{\frac{-5}{3}}, \tag{2.28}$$

where C is the kolmogorov constant, which numerically has been showed to be $C \approx 1.5$ [8].

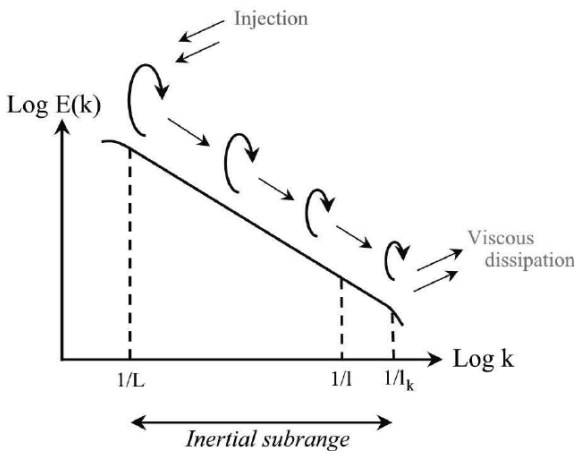

Figure 2.2: A schematic picture of the forward cascade. Energy is injected at small wavenumbers and transfers its energy via the eddies to smaller length scales until viscous forces dissipate the energy.

In the case of an inverse cascade the opposite happens, energy is transferred from smaller to larger scales [3]. The reason for this will be shown in the next section. It should be noted that we will talk about two different types of inverse cascades in this report which often is present together. In order to prevent confusion we refer the inverse cascade that is a direct counterpart to the forward cascade presented in Figure 2.2 as an inverse cascade in the subinertial range and the other type simply as an inverse cascade. In order for the magnetic field to grow an amplification of the seed magnetic field is needed. This can be explained by the contribution of the chiral chemical potential in the induction equation.

2.4 Asymmetry and Chiral chemical potential

The chiral chemical potential μ_5 is a quantum effect that arises from the asymmetry between left- and right-chiral fermions. A seed magnetic field aligns the fermions magnetic moments and in the presence of an asymmetry between the chiral fermions an electric current along the magnetic field is induced [9]. The chiral magnetic effect is illustrated in Figure 2.3, where an asymmetry of massless quarks of positive charge gives rise to the CME current. The setup in this report is somewhat different from the figure but the principles are the same.

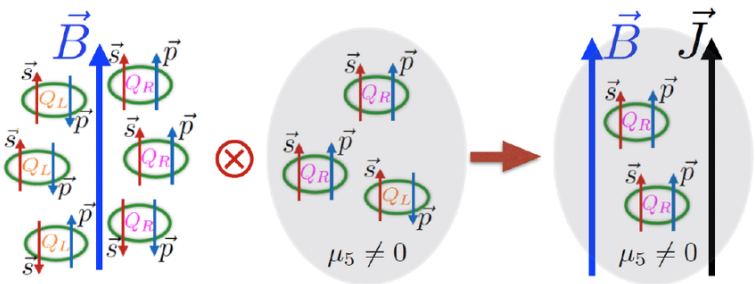

Figure 2.3: Illustration of the chiral magnetic effect. From the left we have an equal number of left-handed and and right-handed massless quarks of positive charge. The two figures on the right shows an asymmetry between left-handed and right-handed quarks which gives rise to a current flowing in the direction of the magnetic field. (Figure credit [2]).

The chiral magnetic effect introduces an additional term in the total current density which leads to a current flowing along the magnetic field, known as the chiral magnetic effect (CME) [9],[3]. The chiral current has the following proportionality,

$$\boldsymbol{J}_{CME} \propto \mu_5 \boldsymbol{B}. \tag{2.29}$$

The standard MHD equtations needs to be modified by the chiral chemical potential which contains another degree of freedom in the form of the number density between the left- and right-chiral fermions[10]. The chiral chemical potential is here defined as,

$$\mu_5 = 24\alpha_{em}(n_L - n_R)(\hbar c/k_B T)^2. \tag{2.30}$$

Where n_L and n_R are the number densities of the fermions, $\alpha_{e_m} \approx 1/137$ is the fine structure constant. It is important to note that this is not a universal definition. Other definitions can be different in sign and in units [11][9][12]. This does not affect our calculations [4]. The chiral induction equation are derived in a similar way as in the standard induction equation. By rewriting and curling Equation (2.4) we obtain,

$$\boldsymbol{\nabla} \times \boldsymbol{E} = \sigma \boldsymbol{\nabla} \times \boldsymbol{J} - \boldsymbol{\nabla} \times (\boldsymbol{u} \times \boldsymbol{B}). \tag{2.31}$$

Now by inserting Faraday's law, Equation (2.1) we get,

$$-\frac{\partial \boldsymbol{B}}{\partial t} = \sigma \boldsymbol{\nabla} \times \boldsymbol{J} - \nabla \times (\boldsymbol{u} \times \boldsymbol{B}). \tag{2.32}$$

It is often convenient for numerical purposes to work with the uncurled version of the induction equation,

$$\frac{\partial \boldsymbol{A}}{\partial t} = \boldsymbol{u} \times \boldsymbol{B} - \eta \boldsymbol{J}_{\text{ohm}}. \tag{2.33}$$

We also have Ampere's law with the total current as,

$$\frac{\partial \boldsymbol{E}}{\partial t} = \boldsymbol{\nabla} \times \boldsymbol{B} - \boldsymbol{J}_{\text{tot}}, \tag{2.34}$$

where we can neglect the change in the electric field as mentioned above. This leads to,

$$\boldsymbol{\nabla} \times \boldsymbol{B} = (\boldsymbol{J}_{\text{ohm}} + \boldsymbol{J}_{\text{CME}}), \tag{2.35}$$

which we can solve for $\boldsymbol{J}_{ohm}$ and insert in Equation (2.33),

$$\frac{\partial \boldsymbol{A}}{\partial t} = \boldsymbol{u} \times \boldsymbol{B} - \eta(\boldsymbol{\nabla} \times \boldsymbol{B} - \boldsymbol{J}_{CME}), \tag{2.36}$$

is the uncurled version of the induction equation [3]. The current is proportional to the magnetic field $J_{CME} \propto \mu_5 B$, as shown in Equation (2.29), which leads to the chiral induction equation on the form [3],

$$\frac{\partial \boldsymbol{A}}{\partial t} = \boldsymbol{u} \times \boldsymbol{B} + \eta(\mu_5 \boldsymbol{B} - \boldsymbol{\nabla} \times \boldsymbol{B}). \tag{2.37}$$

The evolution equation of μ_5 is given by

$$\frac{\partial \mu_5}{\partial t} = -\frac{2}{\lambda}\eta(\mu_5 \boldsymbol{B} - \boldsymbol{\nabla}\times\boldsymbol{B})\cdot\boldsymbol{B} - \boldsymbol{\nabla}\cdot(\mu_5\boldsymbol{u}) + D_5\boldsymbol{\nabla}^2\mu_5 - \Gamma_{f\mu_5}, \tag{2.38}$$

where $\lambda = 3\hbar c(8\alpha_{em}/k_B T)^2$, is the feedback of the magnetic field on μ_5, D_5 is the chiral diffussion and $\Gamma_{f\mu_5}$ is the spin flipping rate and will be neglected in this report [13].

In ideal chiral MHD the total volume averaged chirality is conserved and is given by the relationship,

$$\frac{1}{2}\lambda\langle \boldsymbol{A}\cdot\boldsymbol{B}\rangle + \langle\mu_5\rangle = \text{const} \equiv \mu_{50}. \tag{2.39}$$

This means that when helicity increases, the chiral chemical pontential has to decrease [10]. Equation (2.39) gives us the relationship,

$$\langle \boldsymbol{B}^2\rangle \xi_M \lesssim \mu_{50}/\lambda, \tag{2.40}$$

where ξ_M is the magnetic correlation length. This puts an upper limit on the growth of the magnetic field. The magnetic field saturates due to the feedback of the magnetic field to μ_5, depending on the values of μ_{50} and λ. The dispersion relation is given by [10],

$$\gamma(k) = \eta k(\mu_5 - k). \tag{2.41}$$

A dynamo growth occurs when $k < \mu_5$. From the dispersion relation we can find the k-value of maximum growth, which occurs when $k = \mu_5/2$. The dispersion relation holds as long as the field is weak. There will therefore be a limit of the exponential growth, and an inverse transfer of energy is forced. To understand this inverse transfer of energy that occurs in the subinertial range we introduce two waves with wavenumbers p and q that interacts and produces a new wave k as the corresponding wavenumber[1]. We assume conservation of magnetic energy and magnetic helicity which yields,

$$M_p + M_q = M_k, \tag{2.42}$$

and for magnetic helicity,

$$|H_p| + |H_q| = |H_k|. \tag{2.43}$$

If the field is fully helical we see from Equation (2.26) that we can rewrite Equation (2.42) and eq. (2.43) as,

$$2M_p = p|H_p|, \quad 2M_q = q|H_q|. \tag{2.44}$$

Now the sum of the two yields,

$$|H_p|p + |H_q|q = 2M_k \geq k|H_k|. \tag{2.45}$$

Now by substituting Equation (2.43) in Equation (2.45) we have,

$$|H_p|p + |H_q|q \geq k(|H_p| + |H_q|), \tag{2.46}$$

and by solving for k we get the inequality,

$$k \leq \frac{|H_p|p + |H_q|q}{(|H_p| + |H_q|)}. \tag{2.47}$$

This is the weighted mean of the two waves and we can apply the following inequality,

$$\min(p,q) \leq \frac{|H_p|p + |H_q|q}{(|H_p| + |H_q|)} \leq \max(p,q), \tag{2.48}$$

leading to,

$$k \leq \max(p,q). \tag{2.49}$$

If $p = q$, then $k \leq p = q$. This means that the produced wavenumber always is less or equal to the initial wavenumbers and that the new wavenumber k has to inversely transfer magnetic energy to larger scales, hence the name inverse cascade in the subinertial range[1]. Going back to the initial growth of the magnetic field we can introduce two new characteristic velocities based on μ_5 and λ. We can see that λ^{-1} has dimensions of energy per unit length and μ_5 has dimensions of inverse length. From these velocities we can introduce two regions which will determine the evolution of the magnetic field [3]. The regions are given by,

$$\eta k_1 < v_{\mu_5} < v_\lambda < c_s \qquad \text{Regime I}, \tag{2.50}$$

$$\eta k_1 < v_\lambda < v_{\mu_5} < c_s \qquad \text{Regime II}. \tag{2.51}$$

where,

$$v_\lambda = \mu_5/(\bar{\rho}\lambda)^{1/2}, \tag{2.52}$$

$$v_{\mu 5} = \mu_5 \eta. \tag{2.53}$$

The regimes are separated depending on whether the ratio v_λ/v_{μ_5} is small or large. In the first regime the ratio is large. This means that the feedback λ, of the magnetic field on to μ_5 is negligible. This means that the field will become turbulent for high magnetic Reynolds numbers and a growing subinertial inverse cascade will occur due to the realizability condition, Equation (2.25). This will continue until the saturation values is reached and magnetic energy

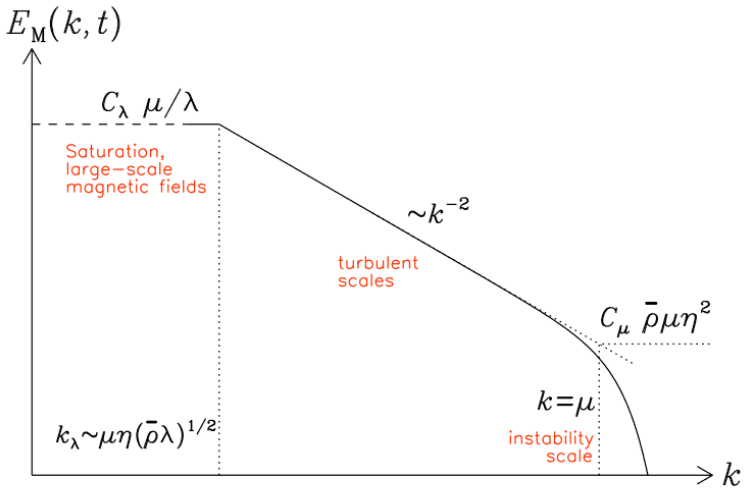

Figure 2.4: The different scales of magnetic energy spectrum driven by the chiral chemical potential. The first region at large wavenumbers is the instability scale where exponential growth occurs followed by the turbulent scale of subinertial inverse cascading and the saturation scale. (Figure credit [3]).

must decay, which can be seen from Equation (2.40). In regime II the ratio will be small, so the feedback on to μ_5 plays an important role and it will prevent the turbulent inverse cascade from growing [3].

From Figure 2.4 we can see the growing turbulent subinertial inverse cascade. The range of turbulent scales, from the instability which occurs at large wavenumbers, to saturation at small k or large lengthscales are often different by many orders of magnitude [3]. This requires models of numerical methods which will be disscussed later.

The energy spectra shown in Figure 2.4 is somewhat different from the standard Kolmogorov theory. The spectrum is here defined as,

$$\int E_M(k,t)dk = \langle \boldsymbol{B}^2 \rangle /2. \tag{2.54}$$

By expressing the magnetic field as an Alfvén velocity [4], $v_A = B/\rho^{1/2}$ and using that $E_M(k,t) \propto d\mathcal{E}_M/dk$, has the dimensions $E_M(k,t) = [\rho][V_A]^2[L]$, gives us $E_M(k,t) = \rho\mu_5\eta^2$ for the initial stage. As opposed to the Kolmogorov spectrum of $k^{-5/3}$ we expect a subinertial range spectrum as k^{-2} as shown in Figure 2.4. In order to obtain the spectra in the subinertial range we can now

use the same arguments as before which leads to,

$$E_M(k,t) = C_{\mu 5}\rho\eta^2\mu_5^3 k^{-2}. \tag{2.55}$$

Where $C_{\mu 5} \simeq 16$ is a Kolmogorov constant obtained from simulations [3]. As stated above, the magnetic field must eventually saturate due to the feedback of the magnetic field on the evolution of μ_5. This can also be realized from Equation (2.40) which leads to,

$$E_M(k,t) \leq C_\lambda \mu_5/\lambda \tag{2.56}$$

where C_λ, like above is another Kolmogorov constant obtained from simulations. In this report we are mostly interested in regime I so we need to find a crossover between the two regions. This can be obtained by introducing a critical value k_λ and by setting Equation (2.55) equal to Equation (2.56),

$$k_\lambda = \sqrt{\rho C_{\mu 5}/C_\lambda}\mu_5\eta, \tag{2.57}$$

which gives us a crossover when $k_\lambda = \mu_5/2$.

2.5 The Hosking integral and Non-helical MHD

The understanding of the decay behaviours of turbulence in hydrodynamics and magnetohydrodynamics has been one of the big challenges in the fields. Kolmogorov formulated the governing invariants that governs the decay behaviour of turbulence in hydrodynamics [7]. Here the conserved quantity is the so called Loitsyansky integral,

$$I_{\boldsymbol{L}} = -\int r^2 \langle \boldsymbol{u}(\boldsymbol{x})\cdot\boldsymbol{u}(\boldsymbol{x}+\boldsymbol{r})\rangle d^3\boldsymbol{r}, \tag{2.58}$$

and it tells us how angular momenta is conserved in the eddies. From dimensional arguments we can obtain the decay law for the kinetic energy. From the Loitsyansky integral we get the dimensions as, U^2L^5. Where U is the velocity and L correlation length. We note that $\tau = L/U$ and in order for Equation (2.58) to be constant, $U^2 \propto L^{-5}$ and $E \propto U^2/2$. By looking at the time evolution of E_K we get,

$$\frac{dE_K}{dt} \sim \frac{-E_K}{\tau} \sim \frac{-E_K^{3/2}}{L} \sim -E_K^{3/2}E_K^{2/10} \sim -E_K^{17/10}, \tag{2.59}$$

leading to [7],

$$E_K \sim t^{-10/7}. \tag{2.60}$$

Which is the decay law of hydrodynamic turbulence. In general we want to find the scaling of the kinetic energy spectrum in terms of power laws in such a way that the decay develops under the an envelope given by,

$$E_K(k,t) \leq C_L I_L k^{\beta}. \tag{2.61}$$

By dimensional arguments in cgs-units, we can find the scaling of the kinetic energy spectrum E_K. We have $E_K = d\mathcal{E}_K/dk$, where $\mathcal{E}_K$ is the kinetic energy with dimensions as $\mathrm{cm}^2\mathrm{s}^{-2}$. Therefore E_K has dimensions of $\frac{\mathrm{cm}^3}{\mathrm{s}^2}$. From Equation (2.61) we therefore have, $\frac{\mathrm{cm}^3}{\mathrm{s}^2} \leq \frac{\mathrm{cm}^7}{\mathrm{s}^2}\frac{1}{\mathrm{cm}^{\beta}}$, which leads to a scaling as $E_K(k,t) \leq C_L I_L k^4$. These arguments will be used later in order to determine the decay behaviours of the magnetic field. The Loitsyansky integral determines the decay and the spectra in the absence of strong correlations. If the long range correlations are present the Saffman integral is the invariant,

$$I_{\boldsymbol{S}} = \int \langle \boldsymbol{u}(\boldsymbol{x}) \cdot \boldsymbol{u}(\boldsymbol{x}+\boldsymbol{r}) \rangle d^3 r. \tag{2.62}$$

Here the physical quantity associated with the Saffman integral is linear momenta. The kinetic energy spectra of the hydrodynamic turbulence will depend on the dominating correlation scales [7]. The kinetic energy spectra is defined as,

$$\mathcal{E}_K(k) = \frac{k^2}{4\pi^2} \int \langle \boldsymbol{u}(\boldsymbol{x}) \cdot \boldsymbol{u}(\boldsymbol{x}+\boldsymbol{r}) \rangle e^{-i\boldsymbol{k}\cdot\boldsymbol{r}} d^3\boldsymbol{r}, \tag{2.63}$$

and by Taylor expanding the spectrum in the limit $\mathcal{E}_k(k \to 0)$ we obtain the spectrum as,

$$\mathcal{E}_K(k \to 0) = \frac{I_{\boldsymbol{S}}}{4\pi^2} k^2 + \frac{I_{\boldsymbol{L}}}{24\pi^2} k^4 + .., \tag{2.64}$$

we can see that if $I_{\boldsymbol{S}} = 0$ we obtain a batchelor spectrum proportional to k^4 and if $I_{\boldsymbol{S}} \neq 0$ we obtain a Saffman spectrum k^2 (See [8] for more details). Since the quantities are conserved the energy spectrum cannot change in the small-k limit, meaning that an inverse transfer of energy is impossible. This was also thought to be the case in non-helical MHD, but recent studies shows that this is not the case. Its important to point out that non-helical MHD does not exclude any helicity, it is the total averaged helicity that is zero, $\langle h_{tot} \rangle = 0$. This means that helicity fluctuations still can be present. Helicity is not a sign definite quantity and if helicity structures with opposite signs merge they will annihilate each other [7].

The evolution of these neutral helical structures is what is conserved in non-helical MHD. A new conserved and finite quantity which is similar to the Loitsyansky and Saffman integral has been introduced and governs the decay

behaviour of magnetic fields in the absence of helicity. The Hosking integral, defined as,

$$I_H = \int \langle h(\boldsymbol{x}) h(\boldsymbol{x}+\boldsymbol{r}) \rangle d^3\boldsymbol{r}. \tag{2.65}$$

The Hosking integral tells us how the evolution of the localized magnetic helical collective structures are conserved. The helicity density h is defined as $h = A \cdot B$. From dimensional arguments we can find the magnetic energy decay law in a similar argument as for the hydrodynamical case. From Equation (2.65) we obtain the dimensions as h^2L^3, where $h = A \cdot B$ and $B = \nabla \times A$ which implies, $A = BL$. This gives us the new scaling $(LB^2)^2L^3$. Finally, $B^4L^5 \sim$ constant. Using that $E_M \sim B^2$, $B^4 \sim L^{-5}$ and $\tau = L/B$ we obtain [7],

$$\frac{dE_M}{dt} \sim \frac{B^2}{L/B} \sim \frac{B^3}{L} \sim \frac{B^3}{B^{-4/5}} \sim B^{19/5} \sim E_M^{19/10}. \tag{2.66}$$

This gives us the decay law of magnetic energy in the absence of total averaged helicity,

$$E_M \sim t^{-10/9}. \tag{2.67}$$

We can also use the same arguments as before in order to get the scaling of the magnetic energy spectrum. From the Hosking integral Equation (2.65) we know that the helicity density has the dimensions $[h] = [B]^2[L]$. From the relationship $E_M = d\mathcal{E}_M/dk$, where $\mathcal{E}_M$ is the magnetic energy and has the dimensions B^2. The magnetic field can again be expressed in terms of an Alfvén velocity. We get the dimensions of the magnetic energy spectra as $\mathrm{cm}^3\mathrm{s}^{-2}$. This leads to the dimensions of helicity density as $[h] = [\mathrm{cm}]^3[\mathrm{s}]^{-2}$. Now the Hosking integral has dimensions as $I_H = [\mathrm{cm}]^9[\mathrm{s}]^{-4}$ [7]. Therefore the dimensions of the magnetic energy spectrum, $E_M \leq C_{I_H} I_H k^\beta$ is on the followig form, $[\mathrm{cm}]^3[\mathrm{s}]^{-2} \leq [\frac{\mathrm{cm}^9}{\mathrm{s}^4}]^{1/2} \frac{1}{\mathrm{cm}^\beta}$, which gives us $\beta = 3/2$. In order to understand the behaviours of the magnetic energy spectra two new quantities is introduced, the magnetic counterpart to the Loitsyansky integral,

$$I_{\boldsymbol{L_M}} \equiv -\int r^2 \langle \boldsymbol{B}(\boldsymbol{x}) \cdot \boldsymbol{B}(\boldsymbol{x}+\boldsymbol{r}) \rangle d^3\boldsymbol{r}, \tag{2.68}$$

where $\boldsymbol{L_M} \equiv \boldsymbol{r} \times \boldsymbol{B}$ and the magnetic Saffman integral is defined as,

$$I_{\boldsymbol{S_M}} \equiv \int \langle \boldsymbol{B}(\boldsymbol{x}) \cdot \boldsymbol{B}(\boldsymbol{x}+\boldsymbol{r}) \rangle d^3\boldsymbol{r}, \tag{2.69}$$

which tells us about the local conservation of magnetic flux. We expect the Saffman integral to be conserved. A similar expansion for the energy spectra as for the hydrodynamic Loitsyansky and Saffman integral can be done, which leads to,

$$\mathcal{E}_M(k \to 0) = \frac{I_{\boldsymbol{S_M}} k^2}{4\pi^2} + \frac{I_{\boldsymbol{L_M}} k^4}{24\pi^2} + ... \tag{2.70}$$

If we assume $I_{SM} = 0$ the Loitsyansky integral with a k^4 spectra will be determining the decay (See [7] for cases when it is different from zero). There is no reason for the magnetic Loitsyansky integral to be conserved in MHD since there is no direct magnetic counterpart to angular momenta. This is one of key argument for the inverse cascade in non-helical MHD. Together with the conserved Hosking integral we obtain,

$$I_{\boldsymbol{L_M}} \sim B^2 L^5 \sim \frac{I_H}{B^2}. \tag{2.71}$$

From Equation (2.71) we can see that when magnetic energy decays $I_{\boldsymbol{L_M}}$ has to increase, leading to an inverse cascade with a k^4 spectra [7]. If I_{SM} is different from zero the Saffman integral with a k^2 spectra will determine the decay. Whether we will see an inverse cascade will depend on if its conserved or not which will be shown later.

We can also find the power law of the correlation length from the conservation of the hosking integral. In order to keep the Hosking integral constant we see that since $E_M \propto t^{-p}$, where $p = 10/9$, the correlation length has to increase in a power law $\xi_M \propto t^q$. From the dimensions of Hosking $\mathrm{cm}^9\mathrm{s}^{-4}$ we get the increase in the correlation length as $\xi_M \propto t^{4/9}$ [7].

2.6 Zero net chirality

In recent studies in the case of zero net chirality, where helicity is balanced by chiral fermions to zero, an adapted version of the Hosking integral seems to determine the decay behaviour of magnetic turbulence at scales large compared to $\mathcal{E}_M$, the correlation length [13]. The adapted Hosking integral is defined as,

$$\mathcal{I}_H(R) = \int_{V_R} \langle h(\boldsymbol{x}) h(\boldsymbol{x}+\boldsymbol{r}) \rangle d^3\boldsymbol{r}, \tag{2.72}$$

where V_R is the volume of a sphere with radius R and the brackets are denoting an average over this volume [13]. Here the total helicity density is defined as, $h_{tot} \equiv A \cdot B + 2\mu_5/\lambda$ which is replaces h in Equation (2.72), meaning $h \to h_{tot}$, which gives us the adapted Hosking integral. The spectra of $h(x)$ is here defined as, $\oint_{4\pi} |\tilde{h}|^2 k^2 d\Omega_k/(2\pi L)^3$, where $d\Omega_k$ is the solid angle in Fourier space and the tilde in, $\tilde{h}$ denotes Fourier space as well (See [13] for more details). The definition of the spectra should satisfy $\int Sp(h)\, dk = \langle h^2 \rangle$. The magnetic energy spectrum is defined as $E_M(k,t) = Sp(B)/2$ which gives us the mean magnetic energy density, $\int E_M\, dk = \langle B^2 \rangle/2$. The mean magnetic helicity spectrum is $\mathcal{H}_M = \int H_M\, dk$, and the correlation length $\xi_M = \mathcal{E}_M^{-1} \int k^{-1} E_M\, dk$.

The growth rate and the dispersion relation is the same here as in the case of finite chirality. The decay behaviour is once again determined from dimensional arguments. But here the argument is somewhat different and a rescaling

of the spectra is used so that, $x \to x' = x\ell$ and time rescales as, $t \to t' = t\ell^{1/q}$. This leads to a decay law of the magnetic correlation length as $\xi_M \propto t^q$ where q has to have the value $q = 4/9$ and $\mathcal{E}_M \propto t^{-p}$ where $p = 10/9$. This means that the $\mathcal{H}_M(t) = -2\mu_5(t)/\lambda \neq 0$ has the same decay behaviours as the Hosking case. In order to understand the decay of helicity we use the real space realazability condition defined as,

$$|\mathcal{H}_M| \leq 2\mathcal{E}_M\xi_M. \tag{2.73}$$

We therefore have the proportionality $|\mathcal{H}_M| \propto \mu_5 \propto t^{-r}$ where $r = p - q = 2/3$.

In the case of zero net chirality we expect the Hosking integral to be conserved which determines the behaviour of the magnetic field[13].

2.7 Shell model

To solve and analyse the cascade behavior the chiral MHD equations we use a cascade or shell model [6]. In the cascade model we assume that the MHD equations are local in Fourier space. The Fourier space is then divided into N-numbers of shells. Where each shell has a coupling to its second nearest neighbour, $2^n \leq k \leq 2^{n+1}$, which allows us to conserve two conservation laws as opposed to the nearest neighbour shell model which can obtain one. This model should be seen as a TOY model and not an actual approximation. It holds similar conservation laws as the MHD equations and has numerically performed very well [14]. The Fourier transform of the velocity field on a length scale of k_n^{-1} is represented by the complex field u_n.

For a general complex velocity field the evolution equation is given by,

$$\frac{du_n}{dt} = i(a_n u^*_{n+1}u^*_{n+2} + b_n u^*_{n-1}u^*_{n+1} + c_n u^*_{n-1}u^*_{n-2}) - \nu k_n^2 u_n. \tag{2.74}$$

The coefficients can be determined from conservation laws and boundary conditions on the shells[6]. Since the model couples to its next nearest neighbours a boundary condition needs to be set so that,

$$\begin{cases} a_n u_{n-2}u_{n-1} = 0, b_n u_{n-1}u_{n+1} = 0, c_n u_{n+1}u_{n+2} \neq 0 & (\text{at } n = 1) \\ a_n u_{n-2}u_{n-1} = 0, b_n u_{n-1}u_{n+1} \neq 0, c_n u_{n+1}u_{n+2} \neq 0 & (\text{at } n = 2) \\ a_n u_{n-2}u_{n-1} \neq 0, b_n u_{n-1}u_{n+1} \neq 0, c_n u_{n+1}u_{n+2} = 0 & (\text{at } n = N-1) \\ a_n u_{n-2}u_{n-1} \neq 0, b_n u_{n-1}u_{n+1} = 0, c_n u_{n+1}u_{n+2} = 0 & (\text{at } n = N) \end{cases} \tag{2.75}$$

Together with energy and helicity conservation,

$$E_K = \frac{1}{2}\sum |u_n|^2, H_K = \frac{1}{2}\sum (-1)^n k_n |u_n|^2, \tag{2.76}$$

we receive the coefficients

$$a = 1/2, b = 1, c = -4. \tag{2.77}$$

In this report we will consider two different cases of the shell model, they all build on the same principle but depending on the formulations of the conservation laws they will differ a bit.

The cascade model in three-dimensional magnetic turbulence has been studied before [14] [15] [16]. The cascade model for a velocity field together with the magnetic field introduces a new Fourier transform of the B-field, B_n with a convolution as,

$$N_n(u,B) = \sum_{i,j=-2}^{2} C_{ij} u_{n+i} B_{n+j}. \tag{2.78}$$

Where the fields takes the form of discrete wave numbers $k_n = 2^n$ where $n = 1, 2, ..., N$. As mentioned above, the conserved quantities plays an important role in both the chiral and non-chiral MHD and in the Shell models. In the first case the shell model and the conserved quantities are defined as,

$$E_{\text{tot}} = \int (\frac{4}{3}\rho_0 v^2 + \frac{1}{2}B^2R^4) d^3x = \text{constant} \tag{2.79}$$

Now using the substitution $b = BR^2$ we obtain

$$\frac{8}{3}\rho_0 \sum_{n=1}^{N} u_n^* \frac{du_n}{d\tilde{t}} + \sum_{n=1}^{N} b_n^* \frac{db_n}{d\tilde{t}} = 0. \tag{2.80}$$

We can now define the evolution equations of the fields,

$$\frac{4}{3}\rho_0 \frac{du_n}{d\tilde{t}} + \nu k_n^2 u_n = N_n(u,b), \tag{2.81}$$

$$\frac{db_n}{d\tilde{t}} + \eta k_n^2 b_n = M_n(u,b). \tag{2.82}$$

In the case of chiral MHD the shell model takes the following form,

$$[\eta k(k_n - (-1)^n \mu_5) + \frac{d}{dt}]B_n = \frac{1}{6} i k_n [M(u,B) - M(B,u)]. \tag{2.83}$$

The fluid density is constant in the shell models, and therefore it is neglected in Equation (2.80) as well as the $4/3$ factor. The shell models for the fields are defined as following,

$$\begin{aligned} 2N_n(u,b) = ik_n(A+C)(u^*_{n+1}u^*_{n+2} - b^*_{n+1}b^*_{n+2}) \\ +ik_n(B-\frac{1}{2}C)(u^*_{n-1}u^*_{n+1} - b^*_{n-1}b^*_{n+1}) \\ -ik_n(\frac{1}{2}B-\frac{1}{4}A)(u^*_{n-2}b^*_{n-1} - b^*_{n-2}u^*_{n-1}), \end{aligned} \tag{2.84}$$

$$\begin{aligned} M_n(u,b) = ik_n(A-C)(u^*_{n+1}b^*_{n+2} - b^*_{n+1}u^*_{n+2}) \\ +ik_n(B+\frac{1}{2}C)(u^*_{n-1}b^*_{n+1} - b^*_{n-1}u^*_{n+1}) \\ -ik_n(\frac{1}{2}B-\frac{1}{4}A)(u^*_{n-2}b^*_{n-1} - b_n n - 2^* u^*_{n-1}). \end{aligned} \tag{2.85}$$

And for chiral MHD we have,

$$M(x,y) = x_{n+1}y_{n+2} + x_{n-1}y_{n+1} + x_{n-2}y_{n-1}. \tag{2.86}$$

Here magnetic helicity is conserved and defined as,

$$H_M = \sum (-1)^n k_n^{-1} |B_n|^2, \tag{2.87}$$

and magnetic energy as,

$$\mathcal{E}_M = \frac{1}{2}\sum_{n=0}^{N} |B_n|^2 \tag{2.88}$$

In a similar procedure as above one obtains the coefficients, $A = 7/5, B = -1/10, C = 1$. This model will be referred to as BEO96 model. Since magnetic helicity is not a sign definite quantity we need to account for this in the calculations. In the BEO96 model positive and negative helicity is assigned to odd and even wavenumbers respectively.

In the other case considered in this report, negative and positive helicity splits and the shell models meaning that we have two separate evolution's, formulated as[17],

$$\begin{aligned} (dv^+_n/dt + \nu k_n^2 v_n +)* = ik_n(v^-_{n+1}v^+_{n+2} + \frac{1-r}{r^2}v^-_{n-1}v^-_{n+1} - \frac{1}{r^3}v^-_{n-1}v^+_{n-2} \\ -b^-_{n+1}b^+_{n+2} - \frac{1-r}{r^2}b^-_{n-1}b^+_{n-2}), \end{aligned} \tag{2.89}$$

$$\begin{aligned} (db^+_n/dt + \eta k_n^2 b^+_n)* = i\frac{k_n}{r(1+r)}(v^-_{n+1}b^+_{n+2} - b^-_{n+1}v^+_{n+2} + v^-_{n-1}b^-_{n+1} - \\ b^-_{n-1}v^-_{n+1} - v^-_{n-1}b^+_{n-2} + b^-_{n-1}v^+_{n-2}), \end{aligned} \tag{2.90}$$

and the model taking account for the negative helicity is defined similarly as,

$$(dv_n^-/dt + \nu k_n^2 v_n -)* = ik_n(v_{n+1}^+ v_{n+2}^- + \frac{1-r}{r^2} v_{n-1}^+ v_{n+1}^+ - \frac{1}{r^3} v_{n-1}^+ v_{n-2}^- \\ -b_{n+1}^+ b_{n+2}^- - \frac{1-r}{r^2} b_{n-1}^+ b_{n-2}^-), \tag{2.91}$$

$$(db_n^-/dt + \eta k_n^2 b_n^-)* = i\frac{k_n}{r(1+r)}(v_{n+1}^+ b_{n+2}^- - b_{n+1}^+ v_{n+2}^- + v_{n-1}^+ b_{n+1}^+ - \\ b_{n-1}^+ v_{n+1}^+ - v_{n-1}^+ b_{n-2}^- + b_{n-1}^+ v_{n-2}^-). \tag{2.92}$$

The evolution of the chiral MHD equations of splitted equations takes the form,

$$[\eta k(k_n \mp (-1)^n \mu_5) + \frac{d}{dt}]B_n^\pm = \frac{1}{6} ik_n [M_\pm(u,B) - M_\pm(B,u)], \tag{2.93}$$

where,

$$M_\pm(x,y) = x_{n+1}^\mp y_{n+2}^\pm + x_{n-1}^\mp y_{n+1}^\mp + x_{n-2}^\pm y_{n-1}^\mp. \tag{2.94}$$

Here the conserved quantities, magnetic energy and magnetic helicity is defined as,

$$\mathcal{E}_M = \sum_{n=0}^{N} (|B_n^+|^2 + |B_n^-|^2), \;\; \mathcal{H}_M = \sum_{n=0}^{N} (|b_n^+|^2 - |b_n^-|^2)/k_n. \tag{2.95}$$

In all of the cases defined above a second order Adams-Bashforth scheme is used for solving the shell models. By rearranging Equation (2.74) and introducing an integrating factor $e^{\nu k_n^2 t}$, we obtain,

$$\frac{du_n}{dt} + \nu k_n^2 u_n = e^{-\nu k_n^2 t} \frac{d}{dt}(u_n e^{\nu k_n^2 t}). \tag{2.96}$$

The equations for BEO96 and BEO97 are solved on the form,

$$\frac{du_n}{dt} + \nu k_n^2 u_n = N_n(t), \tag{2.97}$$

with the modified Adam-Bashforth scheme as,

$$u_n(t+\delta t) = k_n u_n(t) + \\ \frac{1}{2}\delta t[3N_n(t) - K_n N(t-\delta t)]. \tag{2.98}$$

Here $K_n = e^{-\nu k_n^2 \delta t}$ [14].

3. Numerical results

In this report we have studied chiral MHD where we have finite chirality and the volume averaged chirality is conserved. We have also studied the case of zero-net chirality when helicity is balanced to zero by chiral fermions and when the conserved quantity is the Hosking integral and determines the decay behaviours of the magnetic fields. In this case we have used two different models of the shell model which are presented above. The equations of the shell model together with the Navier-stokes equations are already implemented in the PENCIL CODE where we solve the equations. The different decay behaviours are determined by the relevant conservation laws. We have seen their different scaling which is determined from dimensional arguments. Therefore we can test the shell models with similar conservation laws against the scaling of the actual decay laws. In order to test how well the shell models reproduce the decays of the magnetic fields we need to compare with direct numerical simulations.

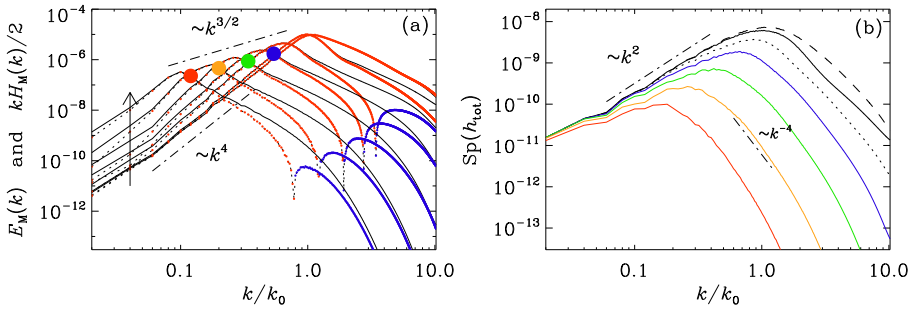

Figure 3.1: Magnetic energy spectra and magnetic helicity spectra plotted in (a), in (b) the magnetic helicity variance spectra is shown for zero net chirality with an initial k^4 spectra. In (a) red and blue dots are positive and negative helicity. The colors determine different times, 1500, 5000, 15 000, 50 000. (Figure credit [4]).

From direct numerical simulations we can see from Figure 3.1 that the inverse cascade develops under the envelope of $k^{3/2}$, indicated by the dashed line. We also see the Loitsyansky integral with a k^4 spectra increasing as magnetic energy decays indicated by the upward arrow. As mentioned earlier this is what we expect when $I_{SM} = 0$ which allows the not conserved Loitsyansky

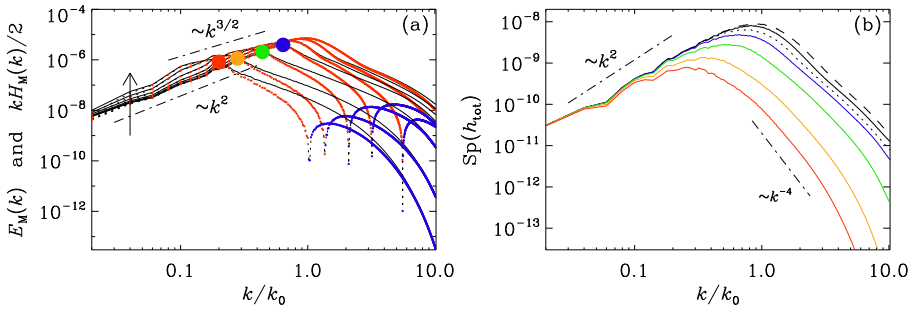

Figure 3.2: Magnetic energy spectra and magnetic helicity spectra plotted in (a), in (b) the magnetic helicity variance spectra is shown for zero net chirality with an initial k^2 spectra. The times are the same as in Figure 3.1. (Figure credit [4]).

integral to push the spectra upwards. On the contrary when $I_{SM} \neq 0$, we expect a k^2 spectra as shown in Figure 3.2, with no inverse cascading. Nevertheless there seems to be an inverse cascade indicated by the arrow. The reason for this is probably due to the fact that there is still strong contributions from the conservation of mean magnetic helicity. Before, we argued that the reason for the absence of an inverse cascade with a k^2 spectra is due to the conservation of the Saffman integral. In Figure 3.3 (a) and (b), we can see that both the Hosking and Saffman integral is indeed conserved.

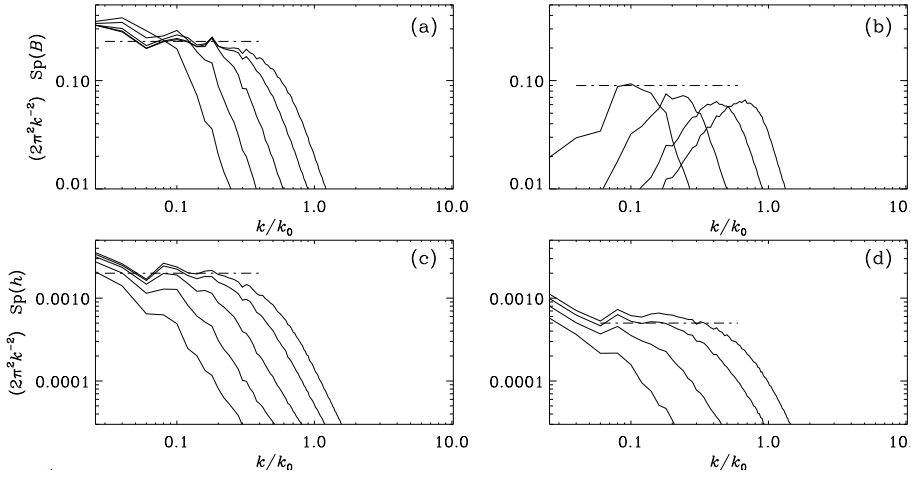

Figure 3.3: Shows the conservation of the Saffman and Hosking integral. The top left figure (a) has an initial k^2 spectra and the right figure (b) has a k^4 spectra. Here $I_{SM} \approx 0.23$ and 0.09 for left and right respectively. The plots (c) and (d) shows the conservation of the Hosking integral with (c) as $I_H \approx 2 \times 10^{-3}$ and 5×10^{-4} in (d) with a k^2 and k^4 spectra for left and right respectively. (Figure credit [4])

In the shell models we have fixed the initial field strength and consider different values of μ_{50} and λ. When $\lambda = 10^{10}$, we have $\mu_{50} = 0.97 \times 10^5$. The decay behaviour of the different quantities are not yet in agreement with what we expect from the Hosking integral. This can be seen from Figure 3.4 where we have used the BEO96 shell model to calculate the slopes (The calculations of the BEO97 model give the same slopes).

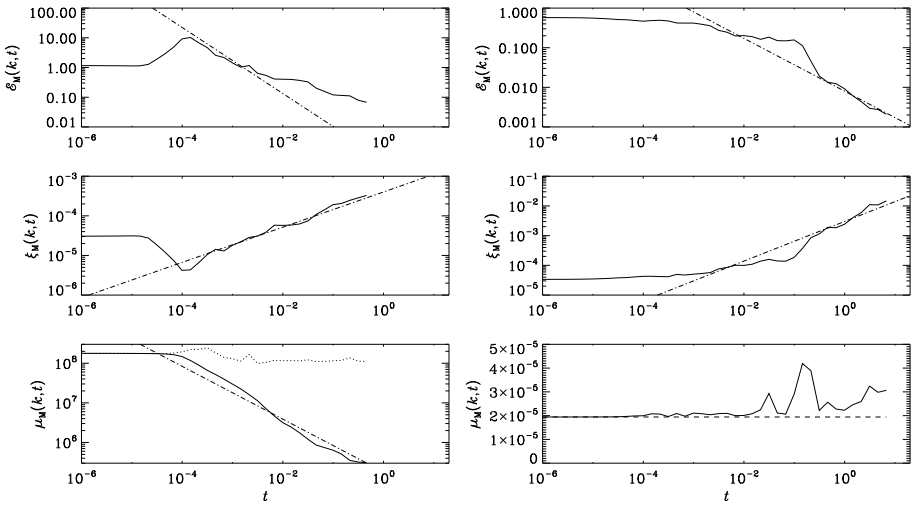

Figure 3.4: The left plot shows the time series of $\mathcal{E}_M(t)$, $\xi_M(t)$, and μ_M for a run with $\lambda = 10^{13}$, $\mu_{50} = 0.97 \times 10^5$, $\eta = 5 \times 10^{-11}$, $\mathcal{E}_M(t)\xi_M(t)\lambda$, BEO96 method, $\delta t = 10^{-8}$. The right figure shows the time series of $\mathcal{E}_M(t)$, $\xi_M(t)$, and μ_M for runs with, $\lambda = 10^{10}$, $\mu_{50} = 0.97 \times 10^5$, $\eta = 5 \times 10^{-11}$, $\mathcal{E}_M(t)\xi_M(t)\lambda$, BEO96 method, $\delta t = 10^{-8}$. The slopes are $p = 2/3$, $q = 2/3$, and $r = 0$ for $\lambda = 10^{10}$ and $p = 10/9$, $q = 4/9$, $r = 2/3$ for $\lambda = 10^{13}$.

Eventually when $\lambda = 10^{13}$, $\mu_{50} = 0.97 \times 10^8$, the slopes are in agreement with what we expect from the conservation of the Hosking integral. By looking at the decay behaviours in Figure 3.4, of the specific parameters we can see how the different values of λ affects the scaling and therefore the conservation of the Hosking integral. So when $\lambda = 10^{13}$ and $\langle h_{tot} \rangle = 0$ we have the scaling as $p = 10/9$, $q = 4/9$ and $r = 2/3$ with a slope of $\beta = 3/2$. Here the shell models is in agreement with the slopes that the conservation of the Hosking integral implies.

From Figure 3.5 we use the shell model to calculate the evolution of the magnetic fields. The fields are here initialized with a k^2 spectrum and with $\lambda = 10^{13}$, $N = 30$ shells, $\nu = \eta = 5 \times 10^{-11}$, and we compute the value of μ_5 as $\mu_5 = -\mu_M$. Here $\mu_M = \mathcal{H}_M \lambda / 2$ is the counterpart of helicity. Wtih the k^2 we expect no inverse cascading. In both of the shell models we see that the Hosking integral is not conserved as the spectra is raising when the magnetic

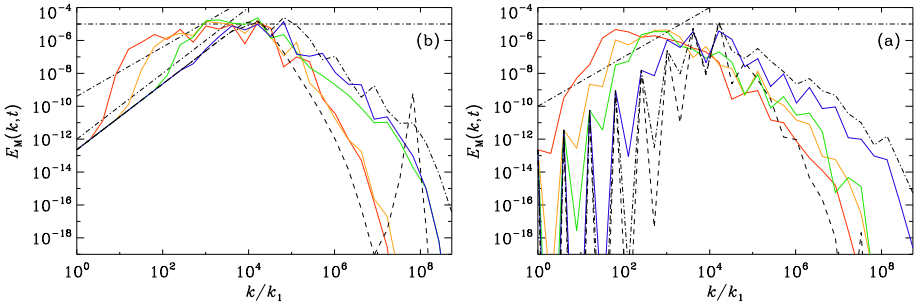

Figure 3.5: Shows the evolution of the magnetic energy $E_M(k,t)$ with with $\lambda = 10^{13}$, calculated with BEO97 and BEO96 for left and right respectively. The different times are indicated by the different colours. Red are 10, orange is 1 and blue is 0.01. The earlier times are denoted by the different dashed black lines.

field decays. We see a clear inverse cascade which we expect not to be possible if I_{SM} is conserved Figure 3.3. The shell models does not seem to capture the same inverse cascade behaviours as the direct numerical simulations does as shown in Figure 3.1 and Figure 3.2. Even if the shell models does not reproduce the expected decay behaviours in the absence of helicity there are other features where the shell model does work as expected. In the case of finite chirality the shell model captures the decay behaviour of the mangetic field. In Figure 3.6 we can see the inverse cascade in the subinertial range with a k^2 spectra and a saturation value at approximately 10^{-6} which can be obtained from Equation (2.56).

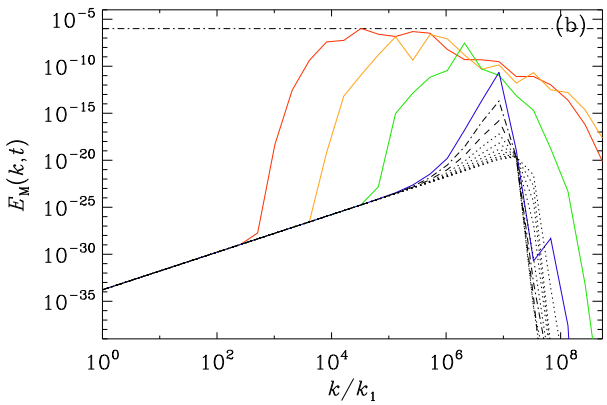

Figure 3.6: Shows the magnetic energy spectra for a run with $\mu_5 = 2^{23} \approx 1.7 \times 10^7$ and with $\eta = 5 \times 10^{-11}$. Calculated with BEO97-model. The different times are indicated by the different colours. Red is 10, orange is 1 and blue is 0.01. The earlier times are denoted by the different dashed black lines.

Comparing the shells models with direct numerical simulations[3], we can see from fig. 3.7 that the evolution of the magnetic field as well as the decay behaviour in fig. 3.6 agrees.

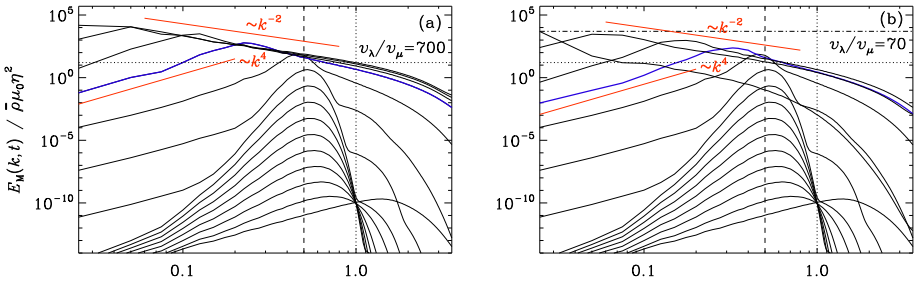

Figure 3.7: Show the evolution of $E_M(k,t)$. The vertical dashed line shows the k-value of maximal growth, $k = \mu_5/2$ and the horisontal line is the saturation value $C_\lambda \mu_5/\lambda$. The ratio v_λ/v_μ is the ratio between the velocity regimes. The ratio implies regime I.(Figure credit [3]).

Therefore the shell models seems to capture the decay behaviour in the finite chiral case. Why the shell models does not not capture the decay behaviours in the Hosking case is still unknown and further studies are required before any conclusions can be drawn.

4. Conclusions

In this report we have studied the importance of magnetic helicity in magnetic turbulence and how the conservation of this quantity leads to a possibility of an inverse cascade due to the realizability condition. We have also explained how the chiral chemical potential causes the induction equation and thereby the magnetic field to grow and inversely cascade in the sub-inertial range. In hydrodynamics the phenomena of an inverse cascade is absent. We explain how the hydrodynamic invariants, the Saffman and Loitsyansky integral prevents the possibility of an inverse cascade. In MHD with an absence of total helicity this was also thought to be the case. The newly introduced Hosking integral as a new conserved quantity in non-helical MHD shows that this is not the case. We also discuss that in the case of chiral MHD, in absence of helicity it also follows the same decay laws as the Hosking integral determines in non-helical MHD. From dimensional arguments we can find the scalings of the magnetic energy spectrum. We study the MHD equations using Shell models to reproduce the evolution of the magnetic field. We compare these results with direct numerical simulations.

The shell models is a powerful tool in capturing the enormous ranges of wavenumbers that the study of decaying MHD turbulence requires. In this report we have seen that the Shell models indeed captures the decay behaviours of the magnetic fields in the case of finite chirality. In the absence of total averaged helicity the shell models does not yet seem to capture the expected decay behaviours. Why this is the case is still unclear and further studies is needed before any conclusions can be drawn. A possibility might also be to introduce a new time stepping scheme of higher order to obtain more precise simulations.

References

[1] AXEL BRANDENBURG AND KANDASWAMY SUBRAMANIAN. **Astrophysical magnetic fields and nonlinear dynamo theory**. *Physics Reports*, **417**(1–4):1–209, Oct 2005. arXiv:astro-ph/0405052. vii, 13, 14, 15, 16, 17, 20, 21

[2] DMITRI KHARZEEV, JINFENG LIAO, S. VOLOSHIN, AND G. WANG. **Chiral Magnetic Effect in High-Energy Nuclear Collisions — A Status Report**. Nov 2015. vii, 18

[3] AXEL BRANDENBURG, JENNIFER SCHOBER, IGOR ROGACHEVSKII, TINA KAHNIASHVILI, ALEXEY BOYARSKY, JURG FROHLICH, OLEG RUCHAYSKIY, AND NATHAN KLEEORIN. **The turbulent chiral-magnetic cascade in the early universe**. *The Astrophysical Journal*, **845**(2):L21, Aug 2017. arXiv:1707.03385 [astro-ph]. vii, viii, 11, 18, 19, 21, 22, 23, 35

[4] AXEL BRANDENBURG AND GUSTAV LARSSON. **Turbulence with Magnetic Helicity that is Absent on Average**. *Atmosphere*, **14**(6):932, May 2023. arXiv:2305.08769 [physics]. vii, viii, 11, 19, 22, 31, 32

[5] ALEXEY BOYARSKY, JUERG FROEHLICH, AND OLEG RUCHAYSKIY. **Self-consistent evolution of magnetic fields and chiral asymmetry in the early Universe**. *Physical Review Letters*, **108**(3):031301, Jan 2012. arXiv:1109.3350 [astro-ph, physics:hep-ph, physics:hep-th]. 11

[6] M. H. JENSEN, G. PALADIN, AND A. VULPIANI. **Intermittency in a cascade model for three-dimensional turbulence**. *Physical Review A*, **43**(2):798–805, Jan 1991. 11, 27

[7] DAVID N. HOSKING AND ALEXANDER A. SCHEKOCHIHIN. **Reconnection-controlled decay of magnetohydrodynamic turbulence and the role of invariants**. *Physical Review X*, **11**(4):041005, Oct 2021. arXiv:2012.01393 [astro-ph, physics:physics]. 11, 23, 24, 25, 26

[8] P. A. DAVIDSON. *Introduction to Magnetohydrodynamics*. Cambridge Texts in Applied Mathematics. Cambridge University Press, Cambridge, 2 edition, 2016. 13, 14, 16, 17, 24

[9] HIROYUKI TASHIRO, TANMAY VACHASPATI, AND ALEXANDER VILENKIN. **Chiral Effects and Cosmic Magnetic Fields**. *Physical Review D*, **86**(10):105033, Nov 2012. arXiv:1206.5549 [astro-ph, physics:hep-ph, physics:hep-th]. 18, 19

[10] IGOR ROGACHEVSKII, OLEG RUCHAYSKIY, ALEXEY BOYARSKY, JÜRG FRÖHLICH, NATHAN KLEEORIN, AXEL BRANDENBURG, AND JENNIFER SCHOBER. **Laminar and Turbulent Dynamos in Chiral Magnetohydrodynamics. I. Theory**. *The Astrophysical Journal*, **846**(2):153, Sep 2017. 19, 20

[11] KOHEI KAMADA, NAOKI YAMAMOTO, AND DI-LUN YANG. **Chiral effects in astrophysics and cosmology**. *Progress in Particle and Nuclear Physics*, **129**:104016, Mar 2023. arXiv:2207.09184 [astro-ph, physics:gr-qc, physics:hep-ph, physics:nucl-th]. 19

[12] ALEXANDER VILENKIN. **Equilibrium parity-violating current in a magnetic field**. *Physical Review D*, **22**(12):3080–3084, Dec 1980. 19

[13] AXEL BRANDENBURG, KOHEI KAMADA, AND JENNIFER SCHOBER. **Decay law of magnetic turbulence with helicity balanced by chiral fermions**. (arXiv:2302.00512), Mar 2023. arXiv:2302.00512 [astro-ph, physics:hep-ph, physics:physics]. 20, 26, 27

[14] AXEL BRANDENBURG, KARI ENQVIST, AND POUL OLESEN. **Large-scale magnetic fields from hydromagnetic turbulence in the very early universe**. *Physical Review D*, **54**(2):1291–1300, Jul 1996. 27, 28, 30

[15] ABHIK BASU, ANIRBAN SAIN, SUJAN K. DHAR, AND RAHUL PANDIT. **Multiscaling in Models of Magnetohydrodynamic Turbulence**. *Physical Review Letters*, **81**(13):2687–2690, Sep 1998. 28

[16] PETER FRICK AND DMITRIY SOKOLOFF. **Cascade and dynamo action in a shell model of magnetohydrodynamic turbulence**. *Physical Review E*, **57**(4):4155–4164, Apr 1998. 28

[17] AXEL BRANDENBURG, KARI ENQVIST, AND POUL OLESEN. **The effect of Silk damping on primordial magnetic fields**. *Physics Letters B*, **392**(3–4):395–402, Jan 1997. arXiv:hep-ph/9608422. 29